



## How to design proper $\pi$ -spacer order of the D- $\pi$ -A dyes for DSSCs? A density functional response

Ji Zhang<sup>b</sup>, Yu-He Kan<sup>a,\*</sup>, Hai-Bin Li<sup>b</sup>, Yun Geng<sup>b</sup>, Yong Wu<sup>b</sup>, Zhong-Min Su<sup>b,\*</sup>

<sup>a</sup> Jiangsu Key Laboratory for Chemistry of Low-Dimensional Materials, School of Chemistry and Chemical Engineering, Huaiyin Normal University, Huaian 223300, PR China

<sup>b</sup> Institute of Functional Material Chemistry, Faculty of Chemistry, Northeast Normal University, Chang Chun, 130024 Jilin, PR China

### ARTICLE INFO

#### Article history:

Received 11 April 2012

Received in revised form

20 May 2012

Accepted 21 May 2012

Available online 27 May 2012

#### Keywords:

Organic dyes

Dye sensitized solar cells

Conjugation order

Vertical dipole moment

Charge recombination

DFT

### ABSTRACT

Three organic donor- $\pi$ -acceptor dyes **1–3** used for dye sensitized solar cells (DSSCs) with difference only in  $\pi$  spacer sequence were investigated via density functional theory (DFT) and time-dependent DFT calculations to shed light on how the  $\pi$  conjugation order influence the performance of the dyes. Key parameters in close connection with the open-circuit photovoltage ( $V_{oc}$ ) and the short-circuit current density ( $J_{sc}$ ), including (i) light harvesting efficiency (LHE); (ii) injection driving force ( $\Delta G_{inject}$ ); (iii) reorganization energy ( $\lambda_{reorg}$ ); (iv) number of photoinjected electrons ( $n_{c,inj}$ ); (v) the extent of charge recombination, and (vi) vertical dipole moment ( $\mu_{normal}$ ), were discussed. The theoretical results reveal that compared with dyes **1** and **2**, dye **3** has the largest  $V_{oc}$  due to its largest  $\mu_{normal}$  and the slowest charge recombination. This conclusion is in good accordance with the experimental results and the theoretical criteria we used would be useful to design and fast screen other organic dyes.

© 2012 Elsevier Ltd. All rights reserved.

### 1. Introduction

Pure metal free organic dye sensitized solar cells (DSSCs) have received significant attention due to the low cost of the raw materials and comparable power conversion efficiency compared to the conventional ruthenium cells [1–11]. So far, DSSCs based on metal-free organic dyes can produce the photo-to-current conversion efficiency ( $\eta$ ) up to 10% under standard AM 1.5 sunlight [12], which is still lower than the crystalline Si-based and inorganic thin film solar cells. Thus, lots of scientists are still working on pure metal-free organic DSSCs to improve their efficiency and thus to realize large-scale commercial production [13–20].

The most extensively studied organic dyes usually adopt the donor- $\pi$  spacer-acceptor (D- $\pi$ -A) structural motif, which exhibit several advantages over coordination complexes: high molar extinction coefficients, low cost of production, and an extraordinary diversity [21]. In this structure, after photoexcitation of the dyes, there would be intramolecular charge transfer from the donor to the acceptor fragment, generating electron-hole separation with the right directionality for posterior electron injection to the conduction band of the semiconductor. In principle, rational and

judicious chemical modification of the individual units, including the donor group, the molecular conductor, and the acceptor group, is desirable to improve the performance of the organic dyes due to their tuned redox and absorption properties. In this context, enormous effects have been devoted to the exploration of various  $\pi$  conjugated spacers in D- $\pi$ -A dyes [16,20,22–25]. Thiophene and its derivatives have been proved to be good  $\pi$  conjugated spacers to boost light harvesting efficiency of the dyes and to be eminent building block commonly used in high-performance carrier transport materials [20,26–29]. At the same time, elongation of the conjugated system is also efficient in broadening the dyes' absorption spectra. Thus, numerous attempts have been devoted to combine these two strategies together to optimize the performance of the dyes maximally. However, this tactic raises an important issue to be resolved, i.e. how to combine the multiple segments of the  $\pi$  conjugation linker to achieve high-performance dyes. Will the topology of  $\pi$  spacer exert dramatic effects on the performance of the dyes, and what extent it is? There is no doubt that the theoretical methods manifest themselves as a reliable and suitable avenue to resolve this problem, saving economical cost and synthesis effort.

In this paper, three organic dyes **1–3** with difference only in  $\pi$  spacer sequence shown in Fig. 1 were investigated through density functional theory (DFT) and time-dependent DFT (TD-DFT) calculations. As shown in Fig. 1, the three dyes have same donor

\* Corresponding authors.

E-mail addresses: [yhkan@yahoo.cn](mailto:yhkan@yahoo.cn) (Y.-H. Kan), [zmsu@nenu.edu.cn](mailto:zmsu@nenu.edu.cn) (Z.-M. Su).

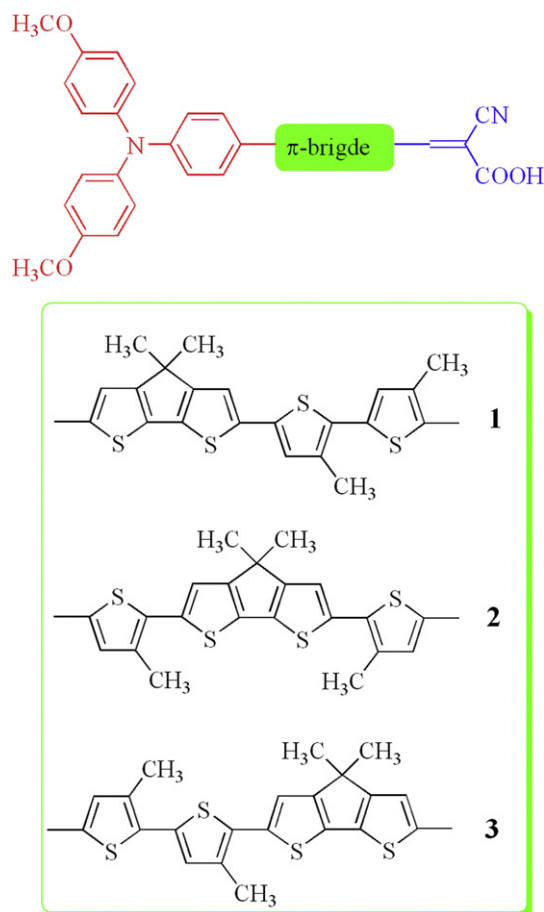


Fig. 1. Molecular structures of studied organic dyes 1–3.

(triphenylamine) and acceptor (2-cyanoacrylic acid) groups, which has proven to be one of the most successful patterns of choice as D and A moieties in D- $\pi$ -A dyes. Two 3-methylthiophene segments and one methyl-substituted cyclopentadithiophene unit with three possible orders were served as  $\pi$ -linker in the dyes. The dyes we studied here are simplified model of **C227**, **C226** and **C225** dyes synthesized by Wang et al., [30] in which the long alkyl chains at  $\pi$ -linker were replaced by methyl groups and the alkoxy groups at the donor were replaced by methoxy groups, which could not affect the electronic properties of the dyes. Theoretical calculations on key parameters controlling the open-circuit photovoltage ( $V_{oc}$ ) and the short-circuit current density ( $J_{sc}$ ) were performed to shed light on how and why the conjugation sequences of the  $\pi$  spacer affect the performance of the dyes. And these parameters are: (i) light harvesting efficiency (LHE); (ii) injection driving force ( $\Delta G_{inject.}$ ); (iii) reorganization energy ( $\lambda_{reorg}$ ); (iv) number of photoinduced electrons transferred from the dye to the semiconductor ( $n_{c,inj}$ ); (v) the extent of charge recombination between the photoinduced electrons in the conduction band of semiconductor and the electron acceptors in the electrolyte, and (vi) vertical dipole moment ( $\mu_{normal}$ ). These theoretical criteria have been successfully used to evaluate the performance of the dyes used in DSSCs [4,31–35]. We hope our work could facilitate the future experimental studies to design and fast screen new efficient organic dyes.

## 2. Computational details

All the calculations were performed with the Gaussian 09 program package [36]. The structure optimization of the ground

state of the dyes before and after binding to  $(TiO_2)_9$  cluster in gas phase have been performed at B3LYP [37] level, 6-31G\* for non-metal atoms while LANL2DZ basis set for Ti atom. Frequency calculations were performed at the same levels of theory as geometry optimization to confirm that the stationary of all the optimized geometries. The optical excitation and absorption spectra of the dyes before and after binding to  $(TiO_2)_9$  cluster were simulated by TD-DFT in conjunction with a conductor-like polarizable continuum model (CPCM) [38,39]. With the aim of checking the reliability, we use a variety of different XC functional, including B3LYP [37], PBE0 [40], BHandHLYP [41], and CAM-B3LYP [42] in TDDFT within the adiabatic approximation to evaluate the effect of different functional on the transition energies on the basis of the optimized ground state structure. Comparison between computational and experimental absorption spectra of the dyes, showed that the results given by the combination of TD-BHandHLYP with 6-31G\* are in good agreement with the experimental values. The natural population analysis (NPA) [43] for organic dyes was performed to reveal the impact of the conjugation order on the  $V_{oc}$  of the cell by evaluating the number of photoinduced electrons in the conduction band. To evaluate dye–iodine interactions, additional DFT calculations were performed by the M06-2X functional [44] using LanL2DZ basis set for I atom and 6-31G\* basis set for other atoms. Basis set superposition error (BSSE) to the binding energies was done by using the counterpoise (CP) method [45,46].

## 3. Results and discussion

### 3.1. Conjugation order effect on the short-circuit current density ( $J_{sc}$ )

To preliminarily appraise the impact of the conjugation order on the  $J_{sc}$ , we first simulated the absorption spectra of the dyes before and after binding to  $(TiO_2)_9$  cluster to compare with the solar spectrum to determine the ability of light harvesting under TD-CPCM-BHandHLYP/6-31G\* for non-metal atoms and LANL2DZ for Ti atom level on the basis of the optimized structures. For the short-circuit current density  $J_{sc}$  in DSSCs, it is determined as:

$$J_{sc} = \int_{\lambda} LHE(\lambda) \Phi_{inject.} \eta_{collect.} d\lambda \quad (1)$$

where  $LHE(\lambda)$  is the light harvesting efficiency related to the oscillator strength ( $f$ ) at a given wavelength. While the larger  $f$ , the stronger LHE, due to the relationship of  $LHE = 1 - 10^{-f}$  [47]. Many theoretical and experimental studies have demonstrated that the dye adsorption process onto the semiconductor is extremely complicated, produces a reorganization of the electronic states. This fact introduces important changes in the electronic absorption spectra. Therefore, it is necessary to consider the semiconductor effect explicitly on the absorption spectra of dyes in the model. Concerning the rationality of the  $TiO_2$  model we adopted, although it may be a little simplification to simulate the effect of the semiconductor fully as compared to the commonly used  $(TiO_2)_{38}$  cluster, Sánchez-de-Armas and Sanz et al. [48–50] have demonstrated it is large enough to reproduce adequately the electronic absorption spectra of some similar dye- $TiO_2$  systems by checking different sizes of  $TiO_2$  clusters. Thus, in view of the good compromise between accuracies and computational efforts, we used the semiconductor model proposed by Sánchez-de-Armas and Sanz et al. to evaluate the influences of semiconductor on absorption spectra and the number of photoinduced electrons. The geometries of the

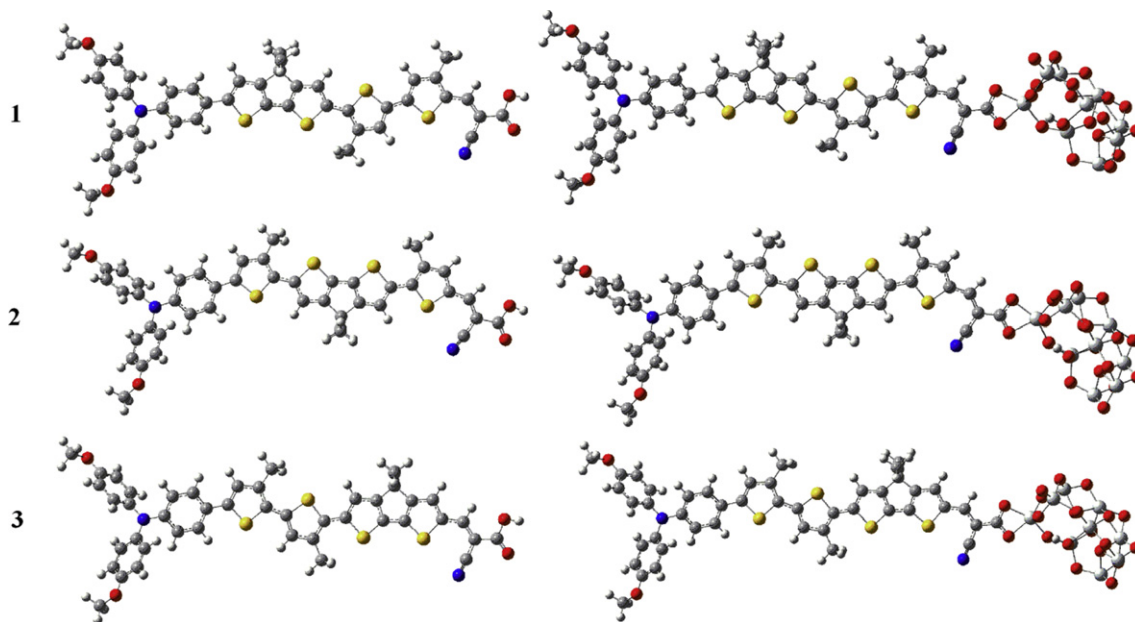


**Fig. 2.** Optimized molecular structures of dyes **1–3** before and after binding to  $(\text{TiO}_2)_9$  cluster in gas phase under B3LYP with 6-31G\* for non-metal atoms and LANL2DZ for Ti atom level.

$(\text{TiO}_2)_9$  cluster was taken from reference [49], and the optimized structures of the free dyes and dye- $(\text{TiO}_2)_9$  clusters are shown in Fig. 2. In addition, as we all know that there are several adsorption configurations possible when the dyes adsorb on the  $\text{TiO}_2$  surface through the  $-\text{COOH}$  group, including molecular adsorption and dissociative adsorption. Fourier transform infrared experiments for the similar systems have demonstrated that carboxylic acid group is deprotonated when the dyes adsorb [51,52]. For dissociative adsorption, including chelating and bridging type, Sánchez-de-Armas and Sanz et al. have also demonstrated that the bidentate chelating adsorption mode is more energetic favorable by geometry optimization of the dyes adsorbed on a  $(\text{TiO}_2)_9$  cluster in both bidentate chelating and bridging configurations for the similar systems [49]. Thus, we adopt this mode to investigate the corresponding properties of the dyes after adsorption.

It is well known that the judicious choice of functional is crucial to describe accurately the absorption of D- $\pi$ -A organic dyes with non-negligible charge transfer (CT) character [15,53,54]. Hence, four different exchange-correlation functionals were tested to see the functional influence on the vertical transition energy of dye **2**, including three hybrid functionals (B3LYP, PBE0 and BHandHLYP) with increasing amount of Hartree-Fock (HF) exchange and long-range-corrected version of B3LYP using the Coulomb-attenuating method (CAM-B3LYP). The calculated results and corresponding experimental values are listed in Table 1. For the hybrid functionals, BHandHLYP which has larger HF exchange (50%) does better than PBE0 (25%) and B3LYP (20%), with the discrepancies of 0.02 eV compared with experiment results. This conclusion is in good agreement with what has been reported by Tretiak and Magyar, i.e. hybrid functionals with large fraction of HF exchange give a good

description of the intramolecular charge-transfer states [55]. On the other hand, the long-range-corrected CAM-B3LYP, which has been widely used to describe the intramolecular charge-transfer states of organic dyes [34], also provide a reliable results with discrepancies of 0.09 eV. Thus, after checking the reliability of a variety of different XC functionals on the transition energies, we adopted the BHandHLYP functional under 6-31G\* level including CPCM solvent effects in the following for investigating optical properties of the three dyes. The calculated maximum absorption wavelengths ( $\lambda_{\text{max}}$ ), oscillator strengths ( $f$ ), light harvesting efficiency (LHE), transition natures, and the corresponding experimental values of dyes **1–3** are summarized in Table 2. It is obvious that the calculated  $\lambda_{\text{max}}$  of the three dyes agrees well with the experimental results with discrepancies by about 0.1 eV. The  $f$  is also in the same trend with the molar extinction coefficient ( $\epsilon$ ), i.e. dyes **1** and **2** have similar  $f$  and smaller than that of dye **3**. This good agreement confirms again the reliability of the used methods. In general, in a real DSSC device, the most commonly used electrolyte is acetonitrile solution, thus, we also simulated the electronic absorption spectra of the dyes in acetonitrile solution to see the solvent effects and the corresponding calculated results are listed in Table S1 (ESI).† Compared with chloroform solution, there is little difference on the electronic absorption spectra of the dyes, no matter on the transition energy or the  $f$  and the main configurations. For the three dyes, the strongest absorption peaks arise from  $S_0 \rightarrow S_1$ , as shown in Fig. S1 (ESI),† which correspond to the dominant promotion of an electron from HOMO to LUMO, together with the minor promotion from HOMO-1 to LUMO. From Table 2 we could find that the conjugation order could have influence on both the CT transition absorption wavelength and corresponding molar extinction coefficient. Fig. 3 shows the frontier molecular orbitals of free dyes **1–3** obtained from CPCM-BHandHLYP/6-31G\* in acetonitrile solution. For these three dyes, the highest occupied molecular orbitals (HOMOs) are spread over triphenylamine and conjugation spacer moiety, whereas the lowest unoccupied molecular orbitals (LUMOs) are mainly localized on conjugation spacer moiety and 2-cyanoacrylic acid fragments. The anchoring group ( $-\text{COOH}$ ) of the three dyes has sizable contributions to the

**Table 1**

The effects of functional on the estimated vertical excitation energy (Ex, eV) of dye **2** with 6-31G\* basis set in chloroform solution.

Functional	CAM-B3LYP	BHandHLYP	PBE0	B3LYP	Exp <sup>a</sup>
Ex	2.27	2.20	1.82	1.69	2.18

<sup>a</sup> Experimental values measured in chloroform solution from Ref. [30].

**Table 2**  
Calculated maximum absorption wavelengths ( $\lambda_{\text{max}}$ ), oscillator strengths ( $f$ ), light harvesting efficiencies (LHE), transition natures and corresponding experimental results of organic dyes in chloroform solution under TD-CPCM-BHandHLYP/6-31G\* level.

Dye	$\lambda_{\text{max}}$ nm/eV	$\lambda_{\text{max}}^a$ nm/eV	$f$	LHE	$\epsilon/\text{M}^{-1} \text{cm}^{-1} (\times 10^4)^a$	Main configurations
1	560/2.22	571/2.17	2.32	0.995	3.92	HOMO–1 $\rightarrow$ LUMO (0.18), HOMO $\rightarrow$ LUMO (0.69)
2	563/2.20	570/2.18	2.31	0.995	4.30	HOMO–1 $\rightarrow$ LUMO (0.18), HOMO $\rightarrow$ LUMO (0.71)
3	547/2.27	545/2.28	2.54	0.997	4.65	HOMO–1 $\rightarrow$ LUMO (0.22), HOMO $\rightarrow$ LUMO (0.67)

<sup>a</sup> Experimental values measured in chloroform solution from Ref. [30].

LUMOs, which could lead to a strong electronic coupling with  $\text{TiO}_2$  surface and thus boost the electron injection efficiency. The frontier molecular orbital spatial distributions indicate that their excited states are of vectorial charge-transfer (CT) transition character, which has been proved to be beneficial for the ultrafast interfacial electron injection from the excited state of the dye to the conduction band (CB) of  $\text{TiO}_2$ , and could also slow down the recombination between the injected electrons in  $\text{TiO}_2$  with the oxidized dye. In view of the multi-configuration character of excited states, the electronic density differences between the ground state and the first excited state were plotted using GaussSum 2.2 [56] (shown in Fig. 3) to assign the character of excited states unambiguously. Obviously, the decreasing electron density mainly localizes on the electronic donor and conjugation spacer segment, while the increasing electron density mainly localizes on the conjugation spacer and electronic acceptor, which is indicative of an intra-molecular CT when the transition occurs, agreeing well with the electronic structure analysis discussed above.

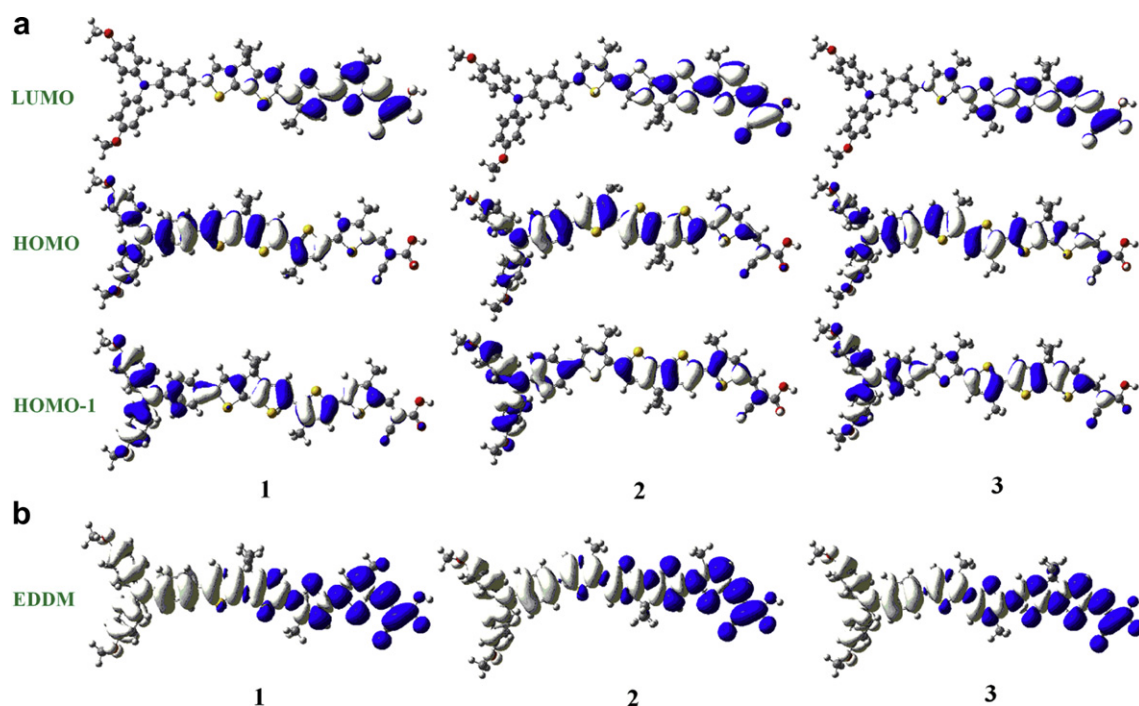
As we all know, the absorption spectrum properties could be affected when the dyes adsorb onto the semiconductor due to the interaction between the dyes and the semiconductor. Compared with the absorption properties of the free dyes, we prefer to get insight into the corresponding properties of the dyes after binding to semiconductor. Thus we also simulated the UV/Vis absorption spectra of the three dyes after binding to  $(\text{TiO}_2)_9$  cluster at the same level of theory for the free dyes except that the LANL2DZ basis set

was used for Ti atom. The results are listed in Table 3. Apparently, after binding, the maximum absorption wavelengths are red shifted, and  $f$  were improved due to the interaction between the dyes and the semiconductor comparing with the free dyes. The electron density difference maps also demonstrate that there are charge transfer from the donor part to the acceptor ( $\text{TiO}_2$ )<sub>9</sub> when transition occurs due to the electron density distributions on the ( $\text{TiO}_2$ )<sub>9</sub> cluster. After binding to the semiconductor, the three dyes have similar LHE as listed in Table 3.

According to the parameters affecting  $J_{\text{sc}}$ , we know that besides the LHE, the electron injection efficiency  $\phi_{\text{inject}}$  could also influence  $J_{\text{sc}}$ , which is closely related to the driving force ( $\Delta G_{\text{inject}}$ ) of the electron injection from the photoinduced excited states of organic dyes to semiconductor surface. In general, the larger  $\Delta G_{\text{inject}}$ , the larger  $\phi_{\text{inject}}$ , and it (in eV) can be expressed as [57]:

$$\Delta G_{\text{inject}} = E^{\text{dye}^*} - E_{\text{CB}} \quad (2)$$

where  $E_{\text{CB}}$  is the reduction potential of the conduction band of the semiconductor, which is sensitive to the conditions, and the experimental value  $-4.00$  eV (vs. vacuum) are widely used [58].  $E^{\text{dye}^*}$  is the excited state oxidation potential of the organic dye. It is generally accepted that the electron injection from the photoinduced excited states of organic dyes to the semiconductor occurs before the vibrational relaxation [59–61]. Hence,  $E^{\text{dye}^*}$  is determined by the redox potential of the ground state of the dye ( $E^{\text{dye}}$ ),

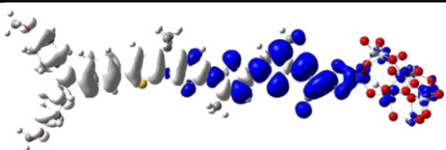
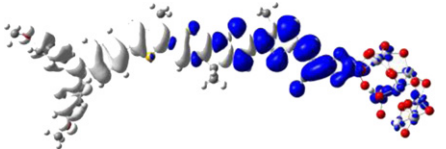
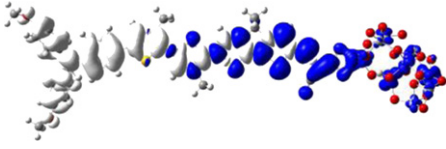


**Fig. 3.** a) Frontier molecular orbitals of free dyes under TD-CPCM-BHandHLYP/6-31G\* level in acetonitrile with isodensity surface of 0.02 au and b) the electronic density differences maps (EDDM) between the ground state and the first excited state with isodensity surface of 0.0002 au.



**Table 3**

Computed maximum absorption wavelengths ( $\lambda_{\text{max}}/\text{nm}$ ), oscillator strengths ( $f$ ), transition natures and the electron density difference maps of dye-(TiO<sub>2</sub>)<sub>9</sub> clusters corresponding to  $S_0 \rightarrow S_1$  in acetonitrile solution under TD-CPCM-BHandHLYP with 6-31G\* for non-metal atoms and LANL2DZ for Ti atom level.

Dyes	Main configurations <sup>a</sup>	$\lambda_{\text{max}}$	$f$	LHE	$S_0 \rightarrow S_1$ <sup>b</sup>
1	HOMO–1 $\rightarrow$ LUMO (0.17) HOMO $\rightarrow$ LUMO (0.70)	617	2.60	0.997	
2	HOMO–1 $\rightarrow$ LUMO (0.20) HOMO $\rightarrow$ LUMO (0.69)	616	2.67	0.998	
3	HOMO–1 $\rightarrow$ LUMO (0.24) HOMO $\rightarrow$ LUMO (0.64)	594	2.96	0.999	

<sup>a</sup> Data in parentheses are main configuration contributions.

<sup>b</sup> The blue represents where the electrons are coming from, and the white represents where the electrons are going.

**Table 4**

Key parameters for deducing  $\Delta G_{\text{inject}}$  and corresponding experimental values ( $V$  vs  $F_c^+/F_c$ ) [30]. The calculated (B3LYP/6-31G\*/acetonitrile) reorganization energies is also reported.

Dyes	$E^{\text{dye}}/\text{eV}$	$\lambda_{\text{max}}/\text{eV}$	$E^{\text{dye}^*}/\text{eV}$	$\Delta G_{\text{inject}}/\text{eV}$	$\lambda_{\text{reorg}}/\text{eV}$
1	4.75 (0.21)	2.01	2.74	–1.26	0.219
2	4.78 (0.24)	2.01	2.77	–1.23	0.206
3	4.82 (0.29)	2.09	2.73	–1.27	0.183

and the vertical transition energy ( $\lambda_{\text{max}}$ ), i.e.  $E^{\text{dye}^*} = E^{\text{dye}} - \lambda_{\text{max}}$  [57]. For  $E^{\text{dye}}$ , it was evaluated at CPCM-(U) B3LYP/6-311G\*\* level with the geometry of optimized organic dyes adsorbed on (TiO<sub>2</sub>)<sub>9</sub> cluster. Here key parameters for deducing  $\Delta G_{\text{inject}}$  and available experimental values are listed in Table 4 to see the conjugation order impacts on the  $\Phi_{\text{inject}}$  of the dyes. We could find that the calculated ground state oxidation has the same trend with the experimental values and these three dyes has similar driving force ( $-\Delta G_{\text{inject}}$ ) as listed in Table 4, i.e. the conjugation order has almost no effects on the driving force. Thus, just from LHE and driving force related to  $J_{\text{sc}}$ , we could expect that the cell based on these three dyes should have similar  $J_{\text{sc}}$  due to the similar LHE and injection driving force. However, the reported  $J_{\text{sc}}$  decrease in the order of **2** (15.1 mA cm<sup>–2</sup>)  $\approx$  **3** (14.0 mA cm<sup>–2</sup>)  $>$  **1** (12.3 mA cm<sup>–2</sup>) [29], dye **1** exhibit smaller  $J_{\text{sc}}$  albeit similar  $J_{\text{sc}}$  and  $\Delta G_{\text{inject}}$  as dye **2** and **3**. On the basis of the Marcus electron transfer theory [62,63], we know that besides the reaction free energy, the reorganization energy  $\lambda_{\text{reorg}}$  could also affect the kinetics of electron injection. The calculated  $\lambda_{\text{reorg}}$  of the three dyes are also listed in Table 4. The largest reorganization energy of dye **1** (0.219 eV) despite the similar

driving force might explain the lower yield of electron injection measured by the time-correlated single photo counting technique in the experiment. Thus we could get a conclusion that the smaller  $J_{\text{sc}}$  of the cell utilizing dye **1** measured in experiment was in part due to its lower yield of electron injection, owing to its largest reorganization energy.

### 3.2. Conjugation order effect on the open-circuit photovoltage ( $V_{\text{oc}}$ )

Concerning the impact of the conjugation order on the  $V_{\text{oc}}$  of the cell, we first calculated the NPA charge distributions of dye-(TiO<sub>2</sub>)<sub>9</sub> at both ground state and first excited state at CPCM/B3LYP/6-31G\* for non-metal atoms and LANL2DZ basis set for Ti atom level using NBO 3.1 implemented in Gaussian 09 to qualitatively or semi-quantitatively determine the number of photoinduced electron ( $n_{\text{c,inj}}$ ) from the excited dye to (TiO<sub>2</sub>)<sub>9</sub>. As for  $V_{\text{oc}}$  in DSSC, it can be determined by [64]:

$$V_{\text{oc}} = \frac{E_c}{q} + \frac{kT}{q} \ln \left( \frac{n_c}{N_{\text{CB}}} \right) - \frac{E_{\text{redox}}}{q} \quad (3)$$

In Eq. (3),  $kT$  and  $q$  are constants, represent the thermal energy and the unit charge, respectively.  $E_{\text{redox}}$  is the electrolyte Fermi-level and  $N_{\text{CB}}$  is the accessible density of conduction band states ( $7 \times 10^{20} \text{ cm}^{-3}$ ) [65]. Here we assume that they are constant, too.  $E_c$  is the conduction band edge of semiconductor, and  $n_c$  is the number of electrons in the conduction band, and can be affected by electron photoinjection and electron recombination in an opposite way. Apparently,  $n_c$  is a key parameter determining  $V_{\text{oc}}$ . The results are listed in Table 5. It is obvious that although they

**Table 5**

Calculated atomic charge distribution (in e) of the donor,  $\pi$  spacer, acceptor and (TiO<sub>2</sub>)<sub>9</sub> of the three dyes after binding with the NBO method under (TD)-CPCM-BHandHLYP with 6-31G\* for non-metal atoms and LANL2DZ for Ti atom level.

Dyes	$S_0$				$S_1$				$\Delta q$
	D	$\pi$	A	(TiO <sub>2</sub> ) <sub>9</sub>	D	$\pi$	A	(TiO <sub>2</sub> ) <sub>9</sub>	
1	0.027	0.284	–0.689	0.378	0.120	0.408	–0.872	0.344	0.034
2	0.035	0.271	–0.685	0.379	0.105	0.415	–0.864	0.344	0.035
3	0.041	0.308	–0.720	0.371	0.109	0.415	–0.865	0.341	0.030

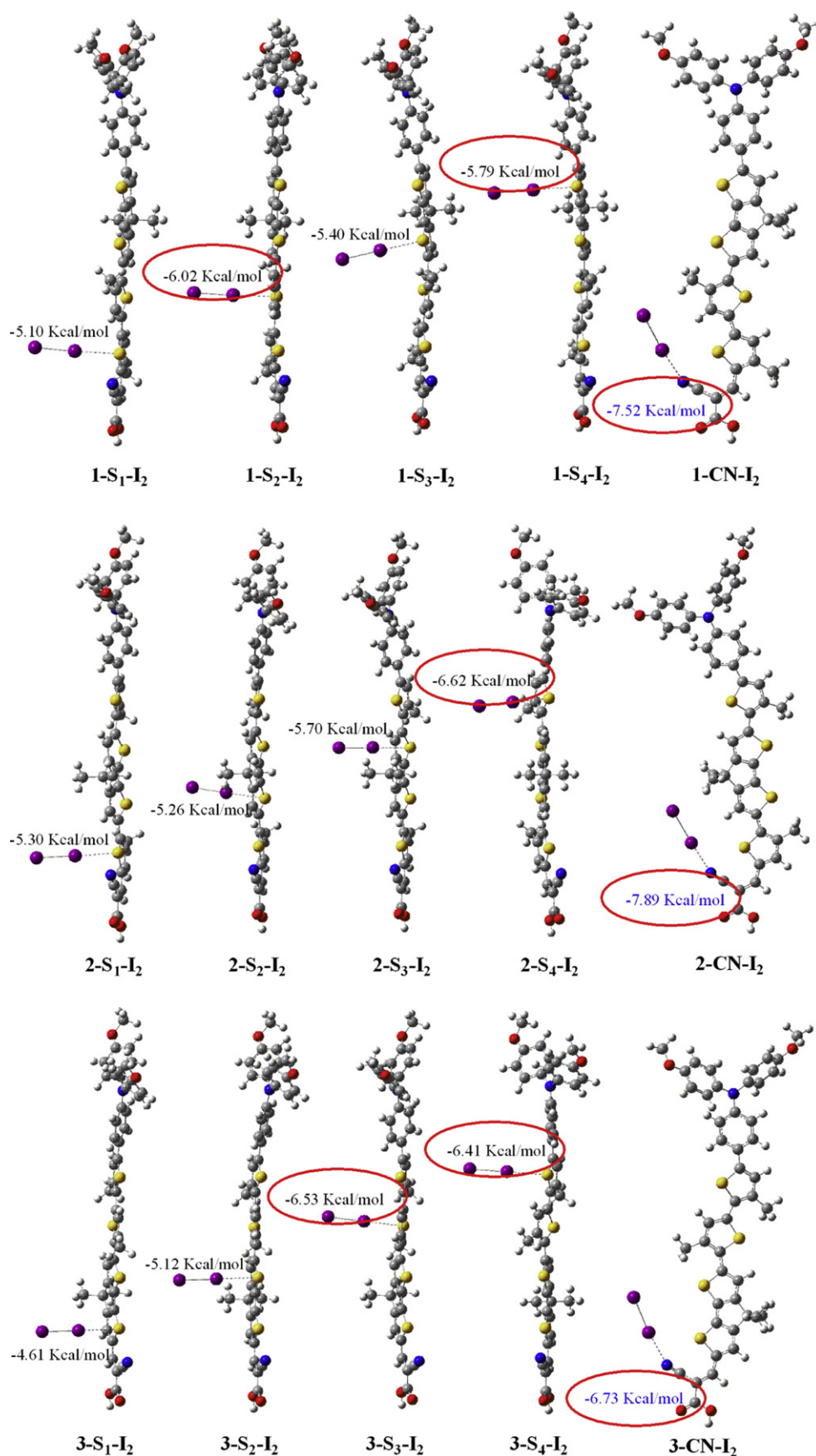


Fig. 4. Optimized molecular structures of the dyes-I<sub>2</sub> complex under M062X/6-31G\* (LANL2DZ basis set for I atom) level.

have different conjugation order, they have similar photoinjected  $n_{c,inj}$ .

However, from the operation mechanism of the cell, we know that the injected electrons in the CB of the semiconductor could also recombine with the oxidized organic dyes and the redox couple in the electrolyte, and the latter one is the main route of electron photovoltage losses [30,66], leading to decreased  $n_c$ , exerting detrimental effect on the  $V_{oc}$ . In order to gain insight into the conjugation order effects on the recombination kinetics of the cell, we also investigated the dye– $I_2$  interaction, which could affect the local concentration of the electron acceptors ( $I_2$ ) near the semiconductor surface. The higher iodine concentration in the vicinity of dye coated  $TiO_2$  surface, the shorter electron lifetime in the CB and thus the more accelerated interfacial charge recombination. Nitrogen and sulfur atoms in the organic dyes could form the halogen bonding through a non-covalent interaction, and the formation of dye– $I_2$  complex has also been reported in the experiment [67]. It is worth noting that  $I_3^-$  could also accept the electrons in the  $TiO_2$  besides  $I_2$ , while Green et al. [68] have demonstrated that the rate of electron recombination with  $I_2$  is 2 order of magnitude faster than with  $I_3^-$ , thus here we consider  $I_2$  as the main electron acceptor for electron combination in the electrolyte. The optimized geometries of the dye– $I_2$  complex under M06-2X/6-31G\* (LANL2DZ basis set for I atom) level [44] in gas phase are listed in Fig. 4. The binding energies, after basis set superposition error (BSSE) correction, of  $I_2$  with different electron donor sites on these molecules were then calculated to determine the preferred binding site and are listed in Fig. 4. For each dye, the S atoms are labeled as  $S_1$ ,  $S_2$ ,  $S_3$  and  $S_4$  in turn from the acceptor toward the donor part. It is obvious although the conjugation order changed, the most preferred binding site for each organic dye is the same, i.e. **dye-CN- $I_2$**  has the largest binding energy for each dye as listed in Fig. 4. For both dye **1** and dye **2**, we could find that the binding energy of **dye-CN- $I_2$**  is significantly larger than that of other site. While for dye **3**, the binding energies of **3- $S_3$ - $I_2$**  (–6.53 kcal/mol) and **3- $S_4$ - $I_2$**  (–6.41 kcal/mol) are slightly smaller than **3-CN- $I_2$**  (–6.73 kcal/mol). It is reasonable to expect that compared with dye **1** and dye **2**, dye **3** should have the smallest iodine concentration around the most preferred binding site (CN), when the dyes were anchored on the semiconductor surface through the carboxyl, because  $S_3$  and  $S_4$  would also like to bond  $I_2$  for the similar binding energies as **3-CN- $I_2$** . In addition, the second preferred binding site

for dye **2** is found to be at  $S_4$  with binding energy being significantly larger than the rest of binding site; while for dye **1**, besides the most preferred binding site CN, sites  $S_2$  (–6.02 kcal/mol) and  $S_4$  (–5.79 kcal/mol) have similar binding energies and are larger than that of  $S_1$  and  $S_3$ . In conclusion, we could expect that the iodine concentration in the vicinity of the most preferred binding site (CN) of dye **1**, where the fast electron recombination between electron in CB and electron acceptor in electrolyte occur, should be smaller as compared to dye **2** because of relative more sites to bind  $I_2$  besides CN. As a result, we could infer that the order of the iodine concentration around the most preferred binding site (CN) among these three dyes is **3** < **1** < **2**. As demonstrated by O'Regan [69], we know that the lifetime of electron in the CB is in the order of dye **3** > dye **1** > dye **2**, which is in excellent agreement with the experimental results (160 ms for **3**, 70 ms for **1** and 22 ms for **2** [30]). Our calculated results suggest that the conjugation order do exert significant influences on the charge recombination. And this strategy has also successfully been used to account for the difference in the lifetime values of two coumarin dyes measured in the experiment by De Angelis et al. [70]. Considering the effect of the charge recombination mentioned above and similar photoinjected  $n_{c,inj}$  collected in Table 5, the  $n_c$  of the three dyes may be in the order of dye **3** > dye **1** > dye **2**.

In light of the equation determining  $V_{oc}$  discussed above, apart from the  $n_c$ ,  $E_c$ , which is sensitive to the condition, can also affect the  $V_{oc}$ . It has been shown that the vertical dipole moment of the adsorbed sensitizer can induce a shift in the conduction band edge of semiconductor. The shift of  $E_c$  is related to the dipole moment of the dye follows as [71]:

$$\Delta E_c = -\frac{q\mu_{normal}\gamma}{\epsilon_0\epsilon} \quad (4)$$

here  $q$  is the electron charge,  $\epsilon_0$  and  $\epsilon$  are the permittivity of the vacuum and the dielectric constant of the organic monolayer.  $\gamma$  is the dye's surface concentration, and  $\mu_{normal}$  is the component of dipole moment of the individual molecule perpendicular to the surface of semiconductor. It is generally accepted that the larger  $\mu_{normal}$  of the adsorbed molecules pointing outward the semiconductor surface, the larger  $V_{oc}$ . In this sense,  $\mu_{normal}$  of the free dyes were calculated under CPCM-B3LYP/6-31G\* level at the geometry of dyes adsorbed onto  $(TiO_2)_9$  cluster. Considering the bidentate binding mode of the dyes, we made the  $C_2$  axis of the

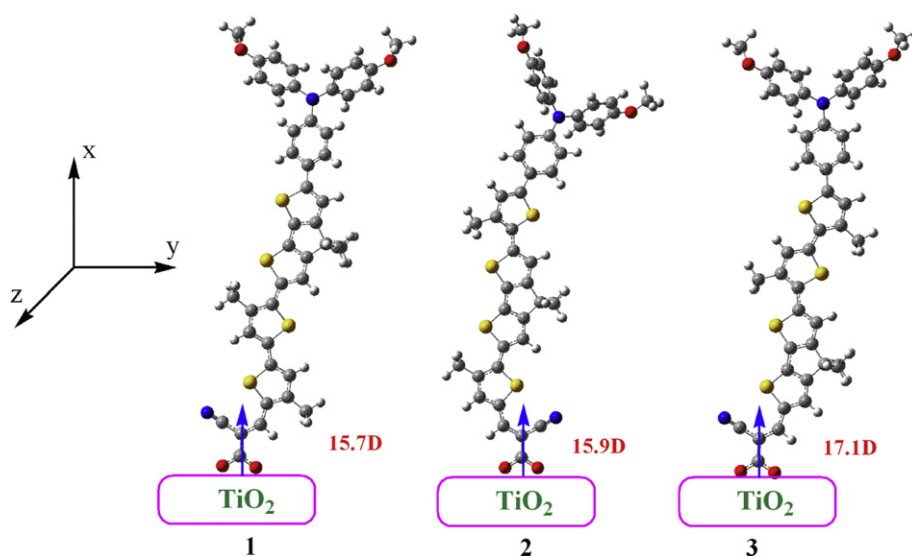


Fig. 5. Calculated vertical dipole moment of dyes **1–3** at CPCM-B3LYP/6-31G\* level in acetonitrile solution. The semiconductor surface is parallel to the  $yz$  plane.

carboxylate in the dye parallel to the *x*-axis, and the semiconductor surface is parallel to the *yz* plane. Thus the orientations of the dyes after binding to semiconductor are simulated. And the dipole moments along *x*-axis of the dyes are referred to as the  $\mu_{\text{normal}}$ . The calculated results are shown in Fig. 5. The  $\mu_{\text{normal}}$  of dyes decrease in the order of **3** (17.1 D) > **2** (15.9 D)  $\approx$  **1** (15.7 D) as the conjugation order changes. Thus combining the parameter determining  $V_{\text{oc}}$ , i.e. vertical dipole moment and the number of electrons in the conduction band, dye **3** should have the largest  $V_{\text{oc}}$  because of its largest  $\mu_{\text{normal}}$  and the slowest charge recombination (*vide supra*), in good agreement with the experimental results (770 mV for dye **3**, 720 mV for dye **2** and 730 mV for dye **1** [30]).

#### 4. Conclusions

The electronic structures, photophysical properties of three organic dyes with only difference in the order of  $\pi$ -conjugation spacer were investigated by DFT and TDDFT methods to see the conjugation effects on the performance of the cell. From our theoretical analysis, we found that for the dyes we studied, the conjugation order had almost no effects on the light harvesting efficiency, the electron injection driving force and the number of photo-injected electrons, but influence the reorganization energy, the vertical dipole moment and the extent of charge recombination between the injected electrons in the conduction band and the electron acceptors in the electrolyte. The smallest  $J_{\text{sc}}$  of dye **1** could be in part ascribed to the largest reorganization energy. On the other hand, the largest vertical dipole moment and the slowest charge recombination lead to the largest  $V_{\text{oc}}$  of dye **3**. These calculated results are in good agreement with the experimental evidence. The soundness of these theoretical criteria used to evaluate the performance of the organic dyes is further confirmed. It also gives us the hint that the charge recombination should also be taken into account besides the widely considered criteria to design and screen of new efficient organic dyes for the experimentalist, saving economical cost and synthesis effort.

#### Acknowledgements

The authors gratefully acknowledge financial support from NSFC (20903020, 21131001), 973 Program (2009CB623605), SRF for ROCS, SEM, the Science and Technology Development Planning of Jilin Province (20090146), The Natural Science Foundation of Jiangsu Province (BK2011408), the Opening Project of Key Laboratory for Chemistry of Low-Dimensional Materials of Jiangsu Province (JSKC10082) and the Cultivation Fund of the Key Scientific Innovation Project of Huaiyin Normal University (11HSGJBZ11).

#### Appendix A. Supplementary material

Supplementary data associated with this article can be found, in the online version, at doi:10.1016/j.dyepig.2012.05.020.

#### References

- [1] Mishra A, Fischer MKR, Bauerle P. Metal-free organic dyes for dye-sensitized solar cells: from structure: property relationships to design rules. *Angew Chem Int Ed* 2009;48:2474–99.
- [2] Zhu W, Wu Y, Wang S, Li W, Li X, Chen J, et al. Organic D-A- $\pi$ -A solar cell sensitizers with improved stability and spectral response. *Adv Funct Mater* 2011;21:756–63.
- [3] Hagfeldt A, Boschloo G, Sun L, Kloo L, Pettersson H. Dye-sensitized solar cells. *Chem Rev* 2010;110:6595–663.
- [4] Preat J, Jacquemin D, Perpète EA. Towards new efficient dye-sensitized solar cells. *Energy Environ Sci* 2010;3:891–904.
- [5] Bai Y, Zhang J, Zhou D, Wang Y, Zhang M, Wang P. Engineering organic sensitizers for iodine-free dye-sensitized solar cells: red-shifted current

- response concomitant with attenuated charge recombination. *J Am Chem Soc* 2011;133:11442–5.
- [6] Horiuchi T, Miura H, Sumioka K, Uchida S. High efficiency of dye-sensitized solar cells based on metal-free indoline dyes. *J Am Chem Soc* 2004;126:12218–9.
- [7] Kim S, Lee JK, Kang SO, Ko J, Yum JH, Fantacci S, et al. Molecular engineering of organic sensitizers for solar cell applications. *J Am Chem Soc* 2006;128:16701–7.
- [8] Nazeeruddin MK, Baranoff E, Grätzel M. Dye-sensitized solar cells: a brief overview. *Solar Energy* 2011;85:1172–8.
- [9] D'Souza F, Ito O. Photosensitized electron transfer processes of nanocarbons applicable to solar cells. *Chem Soc Rev* 2012;41:86–96.
- [10] Ning Z, Fu Y, Tian H. Improvement of dye-sensitized solar cells: what we know and what we need to know. *Energy Environ Sci* 2010;3:1170–81.
- [11] Planells M, Pelleja L, Clifford JN, Pastore M, De Angelis F, Lopez N, et al. Energy levels, charge injection, charge recombination and dye regeneration dynamics for donor-acceptor  $\pi$ -conjugated organic dyes in mesoscopic TiO<sub>2</sub> sensitized solar cells. *Energy Environ Sci* 2011;4:1820–9.
- [12] Zeng W, Cao Y, Bai Y, Wang Y, Shi Y, Zhang M, et al. Efficient dye-sensitized solar cells with an organic photosensitizer featuring orderly conjugated ethylenedioxythiophene and dithienosilole blocks. *Chem Mater* 2010;22:1915–25.
- [13] Tian H, Yang X, Chen R, Zhang R, Hagfeldt A, Sun L. Effect of different dye baths and dye-structures on the performance of dye-sensitized solar cells based on triphenylamine dyes. *J Phys Chem C* 2008;112:11023–33.
- [14] Preat J, Michaux C, Jacquemin D, Perpète EA. Enhanced efficiency of organic dye-sensitized solar cells: triphenylamine derivatives. *J Phys Chem C* 2009;113:16821–33.
- [15] Pastore M, Mosconi E, De Angelis F, Grätzel M. A computational investigation of organic dyes for dye-sensitized solar cells: benchmark, strategies, and open issues. *J Phys Chem C* 2010;114:7205–12.
- [16] Meng S, Kaxiras E, Nazeeruddin MK, Grätzel M. Design of dye acceptors for photovoltaics from first-principles calculations. *J Phys Chem C* 2011;115:9276–82.
- [17] Grätzel M. Dye-sensitized solar cells. *J Photochem Photobiol C Photochem Rev* 2003;4:145–53.
- [18] Liang Y, Peng B, Chen J. Correlating dye adsorption behavior with the open-circuit voltage of triphenylamine-based dye-sensitized solar cells. *J Phys Chem C* 2010;114:10992–8.
- [19] Cai N, Moon S-J, Cevey-Ha L, Moehl T, Humphry-Baker R, Wang P, et al. An organic D- $\pi$ -A dye for record efficiency solid-state sensitized heterojunction solar cells. *Nano Lett* 2011;11:1452–6.
- [20] Liu J, Zhou D, Xu M, Jing X, Wang P. The structure-property relationship of organic dyes in mesoscopic titania solar cells: only one double-bond difference. *Energy Environ Sci* 2011;4:3545–51.
- [21] Casanova D. The role of the  $\pi$  linker in Donor- $\pi$ -Acceptor organic dyes for high-performance sensitized solar cells. *ChemPhysChem* 2011;12:2979–88.
- [22] Cheng X, Sun S, Liang M, Shi Y, Sun Z, Xue S. Organic dyes incorporating the cyclopentadithiophene moiety for efficient dye-sensitized solar cells. *Dyes Pigm* 2012;92:1292–9.
- [23] Duan T, Fan K, Fu Y, Zhong C, Chen X, Peng T, et al. Triphenylamine-based organic dyes containing a 1,2,3-triazole bridge for dye-sensitized solar cells via a 'Click' reaction. *Dyes Pigm* 2012;94:28–33.
- [24] Chang YJ, Watanabe M, Chou P-T, Chow TJ. [2,2]Paracyclophane as a bridging unit in the design of organic dyes for sensitized solar cells. *Chem Comm* 2012;48:726–8.
- [25] Lim K, Kim C, Song J, Yu T, Lim W, Song K, et al. Enhancing the performance of organic dye-sensitized solar cells via a slight structure modification. *J Phys Chem C* 2011;115:22640–6.
- [26] Tian Z, Huang M, Zhao B, Huang H, Feng X, Nie Y, et al. Low-cost dyes based on methylthiophene for high-performance dye-sensitized solar cells. *Dyes Pigm* 2010;87:181–7.
- [27] Shen P, Liu X, Jiang S, Wang L, Yi L, Ye D, et al. Synthesis of new N, N-diphenylhydrazones dyes for solar cells: effects of thiophene-derived  $\pi$ -conjugated bridge. *Dyes Pigm* 2012;92:1042–51.
- [28] Duan Y-A, Geng Y, Li H-B, Tang X-D, Jin J-L, Su Z-M. Theoretical study on charge transport properties of cyanovinyl-substituted oligothiophenes. *Org Electron* 2012;13:1213–22.
- [29] Zhang G, Bai Y, Li R, Shi D, Wenger S, Zakeeruddin SM, et al. Employ a bis-thienothiophene linker to construct an organic chromophore for efficient and stable dye-sensitized solar cells. *Energy Environ Sci* 2009;2:92–5.
- [30] Liu J, Zhou D, Wang F, Fabregat-Santiago F, Miralles SG, Jing X, et al. Joint photophysical and electrical analyses on the influence of conjugation order in D- $\pi$ -A photosensitizers of mesoscopic titania solar cells. *J Phys Chem C* 2011;115:14425–30.
- [31] Zhang J, Li H-B, Sun S-L, Geng Y, Wu Y, Su Z-M. Density functional theory characterization and design of high-performance diarylamine-fluorene dyes with different  $\pi$  spacers for dye-sensitized solar cells. *J Mater Chem* 2012;22:568–76.
- [32] Zhang J, Li H-B, Wu Y, Geng Y, Duan Y-A, Liao Y, et al. TD-DFT studies on phenothiazine-based dyes with different donor in dye-sensitized solar cells. *Chem J Chin U* 2011;32:1343–8.
- [33] Preat J, Jacquemin D, Michaux C, Perpète EA. Improvement of the efficiency of thiophene-bridged compounds for dye-sensitized solar cells. *Chem Phys* 2010;376:56–68.



- [34] Fan W, Tan D, Deng W-Q. Acene-modified triphenylamine dyes for dye-sensitized solar cells: a computational study. *ChemPhysChem* 2012;13: 2051–60.
- [35] Chen J, Bai F-Q, Wang J, Hao L, Xie Z-F, Pan Q-J, et al. Theoretical studies on spectroscopic properties of ruthenium sensitizers absorbed to TiO<sub>2</sub> film surface with connection mode for DSSC. *Dyes Pigm* 2012;94: 459–68.
- [36] Frisch MJ, Trucks GW, Schlegel HB, Scuseria GE, Robb MA, Cheeseman JR, et al. Gaussian 09W, Revision A.02. Wallingford CT: Gaussian, Inc.; 2009.
- [37] Becke AD. Density-functional thermochemistry. III. The role of exact exchange. *J Chem Phys* 1993;98:5648–52.
- [38] Cossi M. Time-dependent density functional theory for molecules in liquid solutions. *J Chem Phys* 2001;115:4708.
- [39] Cossi M, Rega N, Scalmani G, Barone V. Energies, structures, and electronic properties of molecules in solution with the C-PCM solvation model. *J Comput Chem* 2003;24:669–81.
- [40] Perdew JP, Burke K, Ernzerhof M. Generalized gradient approximation made simple. *Phys Rev Lett* 1996;77:3865–8.
- [41] Becke A. A new mixing of Hartree Fock and local density functional theories. *J Chem Phys* 1993;98:1372.
- [42] Yanai T, Tew DP, Handy NC. A new hybrid exchange-correlation functional using the Coulomb-attenuating method (CAM-B3LYP). *Chem Phys Lett* 2004; 393:51–7.
- [43] Foster JP, Weinhold F. Natural hybrid orbitals. *J Am Chem Soc* 1980;102: 7211–8.
- [44] Zhao Y, Schultz NE, Truhlar DG. Design of density functionals by combining the method of constraint satisfaction with parametrization for thermochemistry, thermochemical kinetics, and noncovalent interactions. *J Chem Theory Comput* 2006;2:364–82.
- [45] Boys SF, Bernardi F. The calculation of small molecular interactions by the differences of separate total energies. Some procedures with reduced errors. *Mol Phys* 1970;19:553–66.
- [46] Newton MD, Kestner NR. The water dimer: theory versus experiment. *Chem Phys Lett* 1983;94:198–201.
- [47] Nalwa HS. Handbook of advanced electronic and photonic materials and devices. San Diego, CA: Academic; 2001.
- [48] Sanchez-de-Armas R, Oviedo Lopez JA, San-Miguel M, Sanz JF, Ordejon P, Pruneda M. Real-time TD-DFT simulations in dye sensitized solar cells: the electronic absorption spectrum of Alizarin supported on TiO<sub>2</sub> nanoclusters. *J Chem Theory Comput* 2010;6:2856–65.
- [49] Sanchez-de-Armas R, San Miguel MA, Oviedo J, Sanz JF. Coumarin derivatives for dye sensitized solar cells: a TD-DFT study. *Phys Chem Chem Phys* 2012;14: 225–33.
- [50] Sanchez-de-Armas R, San-Miguel MA, Oviedo J, Marquez A, Sanz JF. Electronic structure and optical spectra of catechol on TiO<sub>2</sub> nanoparticles from real time TD-DFT simulations. *Phys Chem Chem Phys* 2011;13:1506–14.
- [51] Wang Z-S, Hara K, Dan-oh Y, Kasada C, Shinpo A, Suga S, et al. Photophysical and (Photo)electrochemical properties of a coumarin dye. *J Phys Chem B* 2005;109:3907–14.
- [52] Peng B, Yang S, Li L, Cheng F, Chen J. A density functional theory and time-dependent density functional theory investigation on the anchor comparison of triarylamine-based dyes. *J Chem Phys* 2010;132:034305–9.
- [53] Dreuw A, Head-Gordon M. Single-reference ab initio methods for the calculation of excited states of large molecules. *Chem Rev* 2005;105:4009–37.
- [54] Dwyer AD, Tozer DJ. Effect of chemical change on TDDFT accuracy: orbital overlap perspective of the hydrogenation of retinal. *Phys Chem Chem Phys* 2010;12:2816–8.
- [55] Magyar RJ, Tretiak S. Dependence of spurious charge-transfer excited states on orbital exchange in TDDFT: large molecules and clusters. *J Chem Theory Comput* 2007;3:976–87.
- [56] O'Boyle NM, Tenderholt AL, Langner KM. Cclib: a library for package-independent computational chemistry algorithms. *J Comp Chem* 2008;29:839–45.
- [57] Katoh R, Furube A, Yoshihara T, Hara K, Fujihashi G, Takano S, et al. Efficiencies of electron injection from excited N3 dye into nanocrystalline semiconductor (ZrO<sub>2</sub>, TiO<sub>2</sub>, ZnO, Nb<sub>2</sub>O<sub>5</sub>, SnO<sub>2</sub>, In<sub>2</sub>O<sub>3</sub>). *Films J Phys Chem B* 2004;108:4818–22.
- [58] Asbury JB, Wang YQ, Hao E, Ghosh HN, Lian T. Evidences of hot excited state electron injection from sensitizer molecules to TiO<sub>2</sub> nanocrystalline thin films. *Res Chem Intermed* 2001;27:393–406.
- [59] Anderson NA, Ai X, Lian T. Electron injection dynamics from Ru polypyridyl complexes to ZnO nanocrystalline thin films. *J Phys Chem B* 2003;107: 14414–21.
- [60] Ramakrishna G, Singh AK, Palit DK, Ghosh HN. Dynamics of interfacial electron transfer from photoexcited Quinizarin (Qz) into the conduction band of TiO<sub>2</sub> and surface states of ZrO<sub>2</sub> nanoparticles. *J Phys Chem B* 2004;108: 4775–83.
- [61] Zimmermann C, Willig F, Ramakrishna S, Burfeindt B, Pettinger B, Eichberger R, et al. Experimental fingerprints of vibrational wave-packet motion during ultrafast heterogeneous electron transfer. *J Phys Chem B* 2001;105:9245–53.
- [62] Marcus RA. On the theory of electron-transfer reactions. VI. Unified treatment for homogeneous and electrode reactions. *J Chem Phys* 1965;43:679–701.
- [63] Andersen NA, Lian T. Ultrafast electron transfer at the molecule-semiconductor nanoparticle interface. *Annu Rev Phys Chem*; 2005:491–519.
- [64] Marinado T, Nonomura K, Nissfolk J, Karlsson MK, Hagberg DP, Sun L, et al. How the nature of triphenylamine-polyene dyes in dye-sensitized solar cells affects the open-circuit voltage and electron lifetimes. *Langmuir* 2009;26: 2592–8.
- [65] Bai Y, Yu Q, Cai N, Wang Y, Zhang M, Wang P. High-efficiency organic dye-sensitized mesoscopic solar cells with a copper redox shuttle. *Chem Comm* 2011;47:4376–8.
- [66] Green ANM, Palomares E, Haque SA, Kroon JM, Durrant JR. Charge transport versus recombination in dye-sensitized solar cells employing nanocrystalline TiO<sub>2</sub> and SnO<sub>2</sub> films. *J Phys Chem B* 2005;109:12525–33.
- [67] Tuikka M, Hirva P, Rissanen K, Korppi-Tommola J, Haukka M. Halogen bonding—a key step in charge recombination of the dye-sensitized solar cell. *Chem Comm* 2011;47:4499–501.
- [68] Green ANM, Chandler RE, Haque SA, Nelson J, Durrant JR. Transient absorption studies and numerical modeling of iodine photoreduction by nanocrystalline TiO<sub>2</sub> films. *J Phys Chem B* 2004;109:142–50.
- [69] O'Regan BC, Walley K, Juozapavicius M, Anderson A, Matar F, Ghaddar T, et al. Structure/function relationships in dyes for solar energy conversion: a two-atom change in dye structure and the mechanism for its effect on cell voltage. *J Am Chem Soc* 2009;131:3541–8.
- [70] Pastore M, Mosconi E, De Angelis F. Computational investigation of dye–iodine interactions in organic dye-sensitized solar cells. *J Phys Chem C* 2012; 116:5965–73.
- [71] Rühle S, Greenshtein M, Chen SG, Merson A, Pizem H, Sukenik CS, et al. Molecular adjustment of the electronic properties of nanoporous electrodes in dye-sensitized solar cells. *J Phys Chem B* 2005;109:18907–13.